ACS Catalysis

Research Article

pubs.acs.org/acscatalysis

A Highly Effective Catalyst of Sm-MnO_x for the NH_3-SCR of NO_x at Low Temperature: Promotional Role of Sm and Its Catalytic Performance

Dongmei Meng, Wangcheng Zhan,* Yun Guo, Yanglong Guo, Li Wang, and Guanzhong Lu*

Key Lab for Advanced Materials, Research Institute of Industrial Catalysis, East China University of Science and Technology, Shanghai 200237, People's Republic of China

Supporting Information

ABSTRACT: Sm-Mn mixed oxide catalysts prepared by the coprecipitation method were developed, and their catalytic activities were tested for the selective catalytic reduction (SCR) of NO with ammonia at low temperature. The results showed that the amount of Sm markedly influenced the activity of the MnO_x catalyst for SCR, that the activity of the Sm-Mn mixed oxide catalyst exhibited a volcano-type tendency with an increase in the Sm content, and that the appropriate mole ratio of Sm to Mn in the catalyst was 0.1. In addition, the presence of Sm in the MnO_x catalyst can obviously enhance both water and sulfur dioxide resistances. The effect of Sm on the physiochemical properties of the Sm-MnO_x catalyst were investigated by XRD, low-temperature N_2 adsorption, XPS, and FE-SEM techniques. The results showed that the presence of Sm in the Sm-MnO_x catalyst can restrain the crystallization of MnO_x and increase its surface area and the relative content of both Mn^{4+} and surface oxygen (O_S) on the surface of the Sm-MnO_x catalyst. NH_3-TPD, NO-TPD, and in situ DRIFT techniques were used to investigate the absorption of NH_3 and NO on the Sm-MnO_x catalyst and their surface reactions. The results revealed that the presence of Sm in the $Sm_{0.1}$-MnO_x catalyst can increase the absorption amount of NH_3 and NO on the catalyst and does not vary the SCR reaction mechanism over the MnO_x catalyst: that is, the coexistence of Eley−Rideal and Langmuir−Hinshelwood mechanisms (bidentate nitrate is the active intermediate), in which the Eley−Rideal mechanism is predominant.

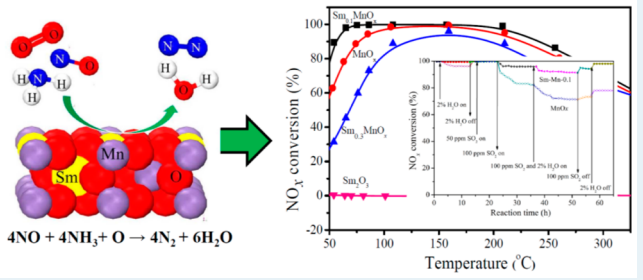

KEYWORDS: *Sm-Mn oxide catalyst, role of Sm, nitrogen oxide, selective catalytic reduction, ammonia reducing agent*

1. INTRODUCTION

Nitrogen oxides (NO, NO_2, and N_2O) resulting from various combustion processes are typical air pollutants, which can cause acid rain, boost the photochemical chain reaction to form photochemical smog, and injure people's respiratory systems directly and the growth of plants. It has been reported that nearly 46% of NO_x emission originates from stationary sources.[1] The selective catalytic reduction of NO_x with ammonia (NH_3-SCR) in the presence of excess oxygen has been considered as one of the best available approaches to control the emission of NO_x produced from the stationary sources such as thermoelectric power plants and incinerators[2] and from mobile sources such as diesel vehicle emission.

Many kinds of catalysts for the NH_3-SCR reaction have been reported, among which commercially available vanadia-based SCR catalysts are one of the most widely used catalysts, due to their high activities at 300−400 °C.[3,4] However, vanadia-based SCR catalysts have some inevitable disadvantages in practical application, such as the narrow operation temperature window, high conversion of SO_2 to SO_3 at high temperature, and the toxicity of vanadium pentoxide to the environment and human health. Other types of promising catalysts that are widely used are transition-metal-exchanged (Cu or Fe) zeolites, which exhibit a wide operation temperature window and satisfactory de-NO_x efficiency.[5−7] However, when the stack gases from stationary sources are purified, the gas temperature is usually low after passing through the sweetener and dust separation plant to eliminate sulfur dioxide and solid particles in the stack gases. The catalytic activities of the previous two kinds of catalysts for the NH_3-SCR reaction are not satisfactory at low temperature. Therefore, there is a great deal of interest in the development of novel SCR catalysts with high activity at low temperature (<300 °C) to control the emission of NO_x from stationary sources.[8,9]

It has been found that some transition-metal oxides have catalytic activity for the low-temperature NH_3-SCR of NO, among which manganese oxides exhibit the highest catalytic performance.[2,10−12] However, the commercial applications of pure MnO_x are restricted severely because of its low surface area and poor thermal stability. Therefore, supported MnO_x

Received: December 24, 2014
Revised: August 19, 2015
Published: September 1, 2015

DOI: 10.1021/acscatal.5b00747
ACS Catal. 2015, 5, 5973−5983

catalysts and Mn-based mixed oxides have attracted more attention, such as MnO_x supported on TiO_2, Al_2O_3, SiO_2, NaY, and AC (activated carbon)[11−17] and Ce−Mn and Cu−Mn mixed oxides.[8,18] With regard to supported MnO_x catalysts, the carrier should possess a high surface area that is beneficial to a better dispersion of active components, and the synergistic reaction between the support and MnO_x should be considered an important factor. For Mn-based mixed oxides, introduction of a secondary element can increase the surface area and defects of MnO_x and improve its structure stability in the operating environment, which is beneficial for the highly efficient adsorption of reactants and long-lasting operation.[19]

Herein, Sm-Mn mixed oxide catalysts were prepared by the coprecipitation method and their catalytic performances for low-temperature NH_3-SCR of NO were investigated, in which the abilities of catalysts for sulfur resistance and H_2O resistance were also estimated, which has not been reported up to now. The effect of Sm addition on the structure and physicochemical properties of MnO_x was systematically investigated by various characterizations. NH_3-TPD, NO-TPD, and in situ DRIFTS techniques were used to study the adsorption of reactants and the surface reaction on the catalysts. On the basis of these results, a highly effective catalyst of Sm-MnO_x for NH_3-SCR of NO_x at low temperature has been achieved, and the promoting mechanism of Sm addition on the MnO_x catalyst was proposed.

2. EXPERIMENTAL SECTION

2.1. Preparation of Catalyst. The Sm-Mn mixed oxide catalysts were prepared by the coprecipitation method. $MnSO_4$ and $Sm(NO_3)_3{\cdot}6H_2O$ were used as the manganese and samarium sources, respectively. Na_2CO_3 solution was used as a precipitator. Typically, the desired amounts of $MnSO_4$ and $Sm(NO_3)_3{\cdot}6H_2O$ were dissolved in deionized water at room temperature. Then this mixed solution and 0.2 M Na_2CO_3 solution were simultaneously dropped into a beaker with stirring and kept at pH 9 for the synthesis. After this solution was stirred for 24 h, the solid product was collected by filtration, dried at 120 °C overnight, and finally calcined in air at 450 °C for 4 h. The catalysts prepared are designated Sm-Mn-*X*, where *X* is the Sm/Mn molar ratio in the synthesis solution. Pure MnO_x was prepared by using the method above without samarium addition.

2.2. Catalyst Characterization. The XRD patterns were recorded on a Brook/D8 diffractometer with Cu Kα radiation (λ 0.154056 nm). The N_2 adsorption−desorption isotherms were measured on a Quantachrome NOVA1200 surface area and pore size analyzer at −196 °C. Prior to measurement, all samples were degassed at 180 °C until a stable vacuum of ca. 5 mTorr was reached. The specific surface area of the sample was calculated by the Brunauer−Emmett−Teller (BET) method. The morphologies of catalysts were investigated by field emission scanning electron microscopy (FE-SEM) images obtained on a NOVA NanoSEM 450 instrument operated at a beam energy of 5 kV. The X-ray photoelectron spectroscopy (XPS) spectra were recorded on a Thermo ESCALAB 250 spectrometer with a monochromatized Al Kα X-ray source (1486.6 eV) and a passing energy of 25 eV. The C 1s peak (binding energy 284.6 eV) of adventitious carbon was used as a reference. The Mn 2p peak and O 1s peak were deconvoluted using XPSPEAK 4.1 with a Shirley background and a convolution of Gaussian and Lorentzian functions (80/20).

Temperature-programmed desorption of NH_3 adsorbed on the catalyst (NH_3-TPD) was carried out on a PX200 apparatus (Tianjin Pengxiang Technology Co. Ltd.) with a thermal conductivity detector (TCD). A 100 mg amount of sample was placed into the quartz reactor and pretreated at 450 °C under a flow of N_2 (50 mL/min) for 1 h. After it was cooled to room temperature, the sample was saturated with a flow of 10% NH_3/N_2 (50 mL/min) for 1 h. Then the sample was flushed by N_2 (50 mL/min) for 1 h and desorption was carried out by heating the sample in N_2 (50 mL/min) from room temperature to 450 °C at 10 °C/min.

NO-TPD was carried out on custom-made equipment with a NO_x analyzer (Thermo Fisher Model 42i-HL NO-NOx-chemiluminescence analyzer). The sample was pretreated in Ar (450 mL/min) at 450 °C for 1 h and cooled to room temperature. Then the sample was exposed to a flow of 500 ppm of NO/Ar (300 mL/min) for 1 h to reach saturated adsorption of NO on the sample, followed by Ar (300 mL/min) purging for 1 h. Finally, NO-TPD was carried out by heating the sample in Ar (300 mL/min) from room temperature to 450 °C at 10 °C/min.

In the experiments of NO and NH_3 oxidation, 300 mg of catalyst (40−60 mesh) was used. For the NO oxidation, the reactant gas was composed of 500 ppm of NO + 5% O_2/95% Ar (300 mL/min). For the NH_3 oxidation a mixed gas of 500 ppm of NH_3 + 5% O_2/95% Ar (300 mL/min) was used. The gas hourly space velocity (GHSV) was about 48600 h^{-1}. The concentration of NO and NO_2 in the tail gas was detected by a Thermo Fisher NO-NO_x-chemiluminescence analyzer. To avoid error caused by the oxidation of ammonia in the converter of the NO/NO_x analyzer, an ammonia trap containing phosphoric acid solution was installed prior to the chemiluminescence detector.

The in situ DRIFT measurements were performed on a Nicolet 6700 FT-IR spectrometer with an MCT detector. In the DRIFT cell with ZnSe windows connected with a gas flow system, the sample was pretreated at 450 °C in Ar for 2 h and then cooled to 50 °C in Ar. The background spectra were recorded at certain temperatures during the cooling process. When the catalyst was kept at a setting temperature, the background spectra were scanned per minute until the final spectrogram could overlap with the last one completely, and the final spectrogram was chosen as the background at this temperature. The background was subtracted from sample spectra collected at the appropriate temperature.

2.3. Catalytic Activity Testing. The catalytic activities of pure MnO_x and Sm-MnO_x for NH_3-SCR in excess oxygen were investigated at atmospheric pressure in a fixed-bed continuous-flow quartz reactor (inner diameter 6 mm). A 300 mg amount of catalyst (40−60 mesh) was used. The reactant gas was composed of 500 ppm of NO, 500 ppm of NH_3, 5% O_2, 2% H_2O (when used), 50 or 100 ppm of SO_2 (when used), and the balance as Ar. The gas hourly space velocity (GHSV) was about 48600 h^{-1}. The concentrations of NO and NO_2 remaining in the reaction gases were analyzed by a Thermo Fisher NO-NO_x-chemiluminescence analyzer. To avoid modest errors caused by the oxidation of ammonia in the converter of the NO/NO_x analyzer, an ammonia trap containing phosphoric acid solution was installed prior to the chemiluminescence detector. NO_x conversion $X(NO_x)$ was calculated as

$$X(NO_x) = \frac{C(NO_x)_{in} - C(NO_x)_{out}}{C(NO_x)_{in}}$$

DOI: 10.1021/acscatal.5b00747
ACS Catal. 2015, 5, 5973−5983

$C(NO_x)_{in}$ and $C(NO_x)_{out}$ denote the concentrations of NO_x in the inlet and outlet, respectively.

3. RESULTS AND DISCUSSION

3.1. Effect of Sm Amount on the Catalytic Activity of Sm-Mn−O Catalyst. The catalytic activities of the Sm-MnO_x, Sm_2O_3, and MnO_x catalysts for the NH_3-SCR reaction are shown in Figure 1. The results showed that pure Sm_2O_3 was

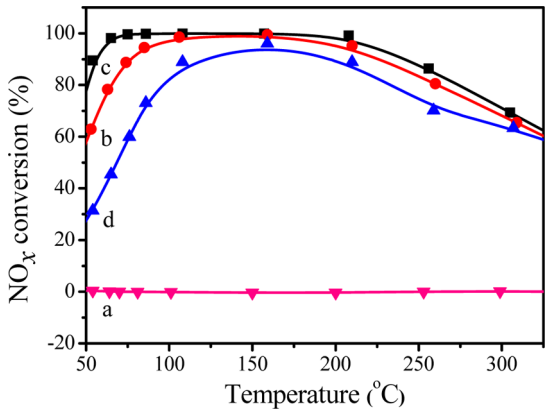

Figure 1. NO_x conversion as a function of the reaction temperature in the NH_3-SCR reaction over (a) Sm_2O_3, (b) MnO_x, (c) Sm-Mn-0.1, and (d) Sm-Mn-0.3 catalysts. Reaction conditions: 0.3 g of catalyst, reactant gas 500 ppm of NO/500 ppm of NH_3/5% O_2/Ar balance, GHSV = 48600 h^{-1}.

almost inactive for the NH_3-SCR reaction at 50−300 °C, and pure MnO_x exhibited a high catalytic activity, over which ∼55% NO_x conversion was achieved at 50 °C and ∼97% NO_x was reduced at ∼100 °C. After Sm was introduced into MnO_x, the activity of the Sm-MnO_x catalyst exhibited a volcano-type tendency with an increase in the Sm content. When Sm/Mn was 0.1 (mol) in the Sm-Mn-0.1 catalyst, the temperature for 100% NO_x conversion was decreased to ∼75 °C and the operation temperature window was greatly enlarged. However, when Sm/Mn was 0.3 in the Sm-Mn-0.3 catalyst, its catalytic activity for the NH_3-SCR reaction was even lower than that over pure MnO_x catalyst.

3.2. Physicochemical Properties of Sm-MnO_x Catalysts. Figure 2 shows the XRD patterns of the MnO_x and Sm-MnO_x catalysts. In the XRD pattern of MnO_x, there were mainly the diffraction peaks of MnO_2 and Mn_5O_8. For the Sm-

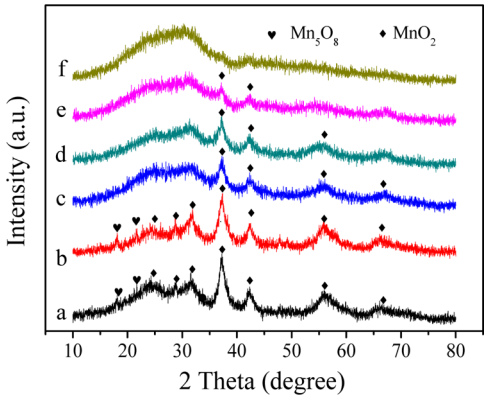

Figure 2. XRD patterns of (a) MnO_x, (b) Sm-Mn-0.01, (c) Sm-Mn-0.03, (d) Sm-Mn-0.05, (e) Sm-Mn-0.1, and (f) Sm-Mn-0.3 catalysts.

MnO_x catalysts, there were only the diffraction peaks of MnO_x and diffraction peaks of Sm species could not be observed, which clearly indicated that the Sm ions were well-dispersed in MnO_x. With an increase in the Sm amount in MnO_x, the intensities of MnO_2 diffraction peaks decreased greatly and the diffraction peaks of Mn_5O_8 disappeared gradually. For the Sm-Mn-0.3 catalyst, no distinct diffraction peak could be observed except a broad bump, implying that this catalyst is poorly crystallized. These XRD results indicated that the introduction of Sm can restrain the crystallization of MnO_x.

Figure 3 shows the SEM images of MnO_x and Sm-MnO_x catalysts. As shown in Figure 3, the shape of MnO_x was the agglomerated bulk with the spherical particles, and the Sm-Mn-0.1 catalyst consisted mainly of the separated spheres along with a spot of stubs. When the Sm content was further increased in the catalyst, such as in the Sm-Mn-0.3 catalyst, although some separated spheres still remained, a large matrix constituted with amorphous particles could be observed.

The BET surface areas of the catalysts are given in Table 1. The Sm-Mn-0.1 catalyst possessed a surface area (135 m^2/g) higher than that of MnO_x (97 m^2/g), because of the high dispersity of the Sm-Mn-0.1 spherical particles. The BET surface area of the Sm-Mn-0.3 catalyst was 105 m^2/g due to the formation of a large matrix. The results above show that the introduction of a certain amount of Sm in the MnO_x catalyst can modulate the particle shape of MnO_x and increase its surface area, which are beneficial to improving the catalytic activity of MnO_x for the SCR reaction.

Figure 4 shows the XPS Mn 2p and O 1s spectra of the MnO_x, Sm-Mn-0.1, and Sm-Mn-0.3 catalysts. The surface atom concentrations of Sm, Mn, and O are summarized in Table 1. In comparison with the molar ratio of Sm/Mn in the bulk, its ratio in the surface was much higher, showing an enrichment of Sm ions on the surface. The Mn 2p peaks could be deconvoluted to three peaks for three samples (Figure 4A); the peaks at 641 ± 0.2 and 642.3 eV represented Mn^{3+} and Mn^{4+}, respectively, and the peak at 643 eV was the satellite peak of manganese.[20,21] The Mn^{4+}/Mn^{3+} atomic ratio (Table 1) was calculated from XPS spectra using XPSPEAK 4.1. It is interesting that the Mn^{4+}/Mn^{3+} atomic ratio increased to 2.31 for the Sm-Mn-0.1 catalyst and decreased to 1.77 for the Sm-Mn-0.3 catalyst, in comparison with Mn^{4+}/Mn^{3+} = 0.69 of the MnO_x catalyst. This is because Sm easily inserted into the defects of MnO_x and the presence of Sm can inhibit the diffusion of Mn^{n+} and O^{2+} ions and prevent the transition from Mn^{4+} to Mn^{3+}, resulting in the high Mn^{4+}/Mn^{3+} atomic ratio in the Sm-MnO_x catalyst.[22]

As shown in Figure 4B, two peaks can be distinguished in the XPS O 1s spectra of MnO_x and Sm-MnO_x catalysts. The peak at ∼529.5 eV was assigned to the lattice oxygen O^{2-} (O_L),[18,23] and the peak at 531.5 eV was assigned to the surface oxygen (Os), including surface-adsorbed oxygen (such as O_2^{2-} or O^-) belonging to defect oxide and hydroxyl-like groups.[24,25] The $O_S/(O_L + O_S)$ ratios for the Sm-MnO_x catalysts were calculated and are shown in Table 1. It is interesting that the $O_S/(O_L + O_S)$ ratios of Sm-MnO_x catalysts are higher than that for pure MnO_x (26.3%); in particular, for the Sm-Mn-0.1 catalyst its $O_S/(O_L + O_S)$ ratio reaches 58.4%, indicating that the Sm-MnO_x catalysts possess more surface oxygen than MnO_x.

The results above show that the Sm-MnO_x catalysts possess a higher Mn^{4+}/Mn^{3+} surface atomic ratio and more surface oxygen species than the MnO_x catalyst, which can enhance the oxidizing power and promote the oxidation of bridged nitrite

DOI: 10.1021/acscatal.5b00747
ACS Catal. 2015, 5, 5973−5983

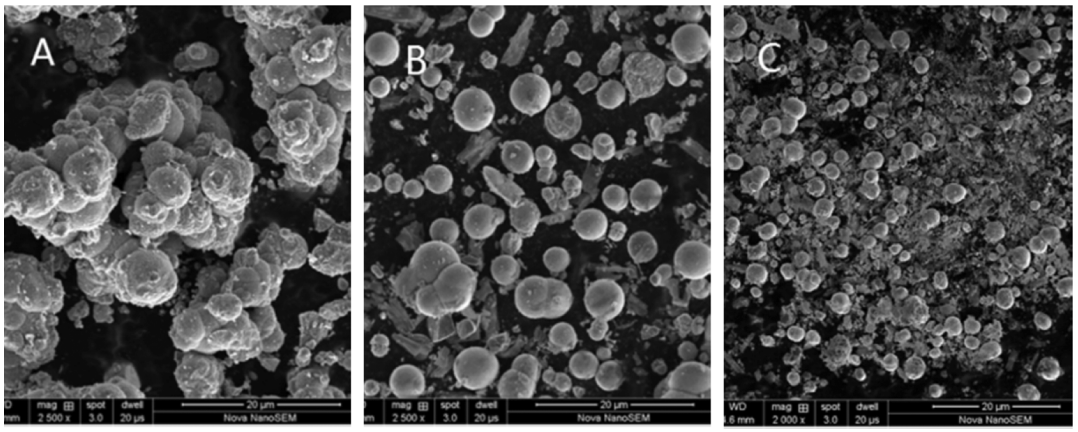

Figure 3. SEM images of (A) MnO_x, (B) Sm-Mn-0.1, and (C) Sm-Mn-0.3 catalysts.

Table 1. BET Surface Area (S_{BET}) and Surface Atom Concentrations of the MnO_x, Sm-Mn-0.1, and Sm-Mn-0.3 catalysts

			surface atom concn[b]			
catalyst	Sm/Mn[a]	S_{BET} (m^2/g)	Sm/Mn	O/Mn	$O_S/(O_L + O_S)$	Mn^{4+}/M^{3+}
MnO_x		97		2.16	26.3%	0.69
Sm-Mn-0.1	0.09	135	0.31	4.26	58.4%	2.31
Sm-Mn-0.3	0.27	105	0.91	6.17	42.3%	1.77

[a]Mole ratio of Sm/Mn determined by ICP analysis. [b]Detected by XPS analysis.

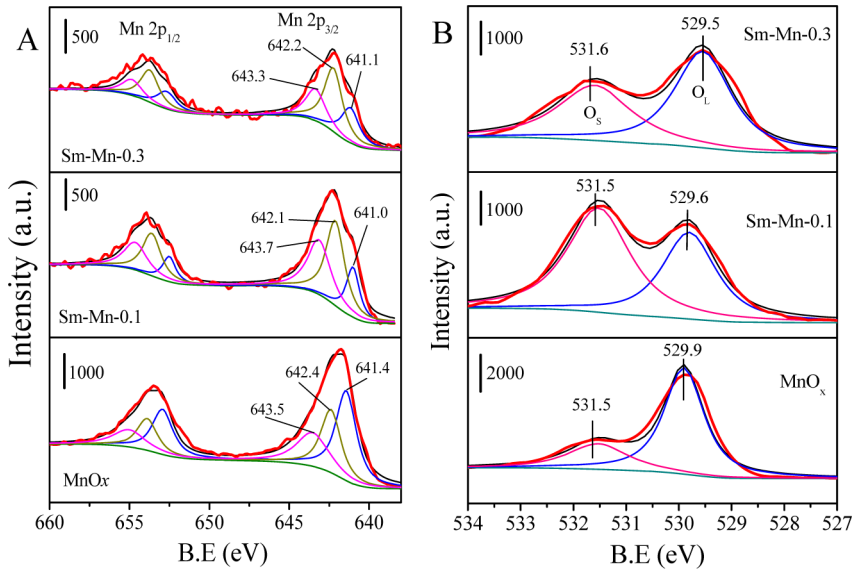

Figure 4. XPS (A) Mn 2p and (B) O 1s spectra of the MnO_x, Sm-Mn-0.1, and Sm-Mn-0.3 catalysts.

adsorbed on the Sm-MnO_x catalyst surface to bidentate nitrate. This will be discussed in detail in section 3.5.

3.3. Temperature-Programmed Desorption. Figure 5 shows the NH_3-TPD profiles of the MnO_x, Sm-Mn-0.1, and Sm-Mn-0.3 catalysts, in which there is only one broad desorption peak at 50−300 °C and the positions of their desorption peaks or top temperatures are not obviously different. In addition, the peak area of the Sm-Mn-0.1 catalyst is slightly larger than that of the other two catalysts, which should be ascribed to its larger surface area and greater number of Lewis acid sites (confirmed by in situ DRIFT results). In general terms, the effect of adding Sm on the surface acidic properties of MnO_x catalyst is not obvious.

The NO-TPD profiles of the catalysts are also shown in Figure 5. Different from the NH_3-TPD results, the NO_x desorption profile on the MnO_x catalyst has obviously changed after adding Sm. In the NO-TPD curve of the MnO_x catalyst, there are two obvious NO_x desorption peaks at 103 and 400 °C with a shoulder desorption peak at 170 °C. In comparison with the in situ DRIFTS results of NO adsorbed on the MnO_x and Sm-Mn-0.1 catalysts (Figures S1 and S2 in the Supporting Information) at different temperatures, the peak below 150 °C can be attributed to physisorbed NO_x and the decomposition of monodentate nitrate species and bridged nitrite and the peak above 150 °C is due to the decomposition of bridged nitrate species and bidentate nitrate species with higher thermal stability.[26] For the Sm-Mn-0.1 and Sm-Mn-0.3 catalysts, in

DOI: 10.1021/acscatal.5b00747
ACS Catal. 2015, 5, 5973−5983

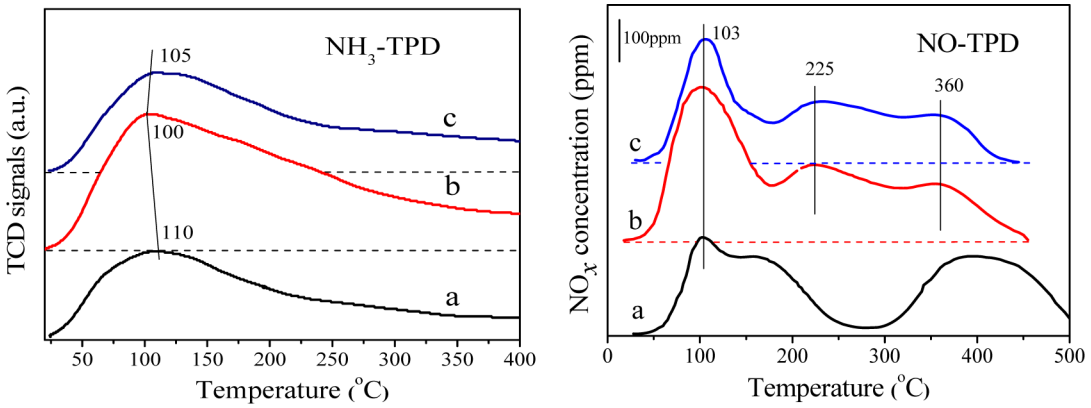

Figure 5. NH_3-TPD and NO-TPD profiles of (a) MnO_x, (b) Sm-Mn-0.1, and (c) and Sm-Mn-0.3 catalysts.

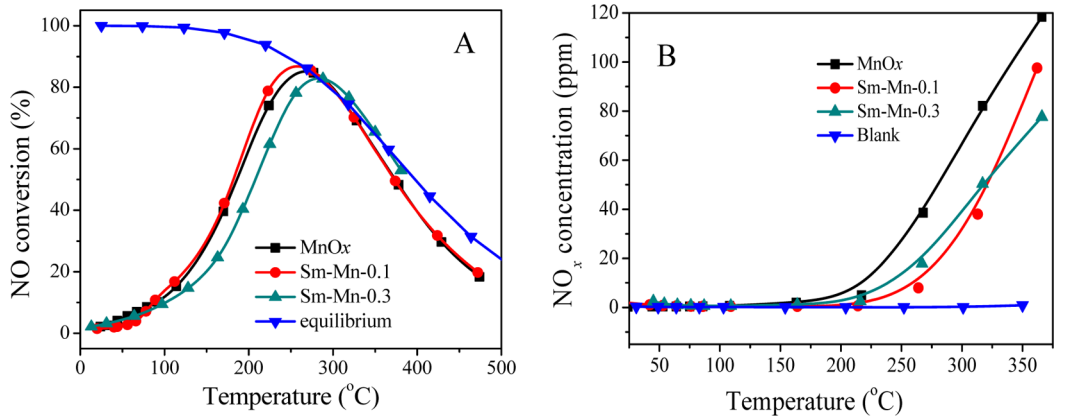

Figure 6. (A) NO conversion in separate NO oxidation reactions and (B) NO_x concentration produced in separate NH_3 oxidation reactions over different catalysts. Reaction conditions: 500 ppm of NO or 500 ppm of NH_3, 5 vol % O_2, Ar balance, total flow rate 300 mL/min.

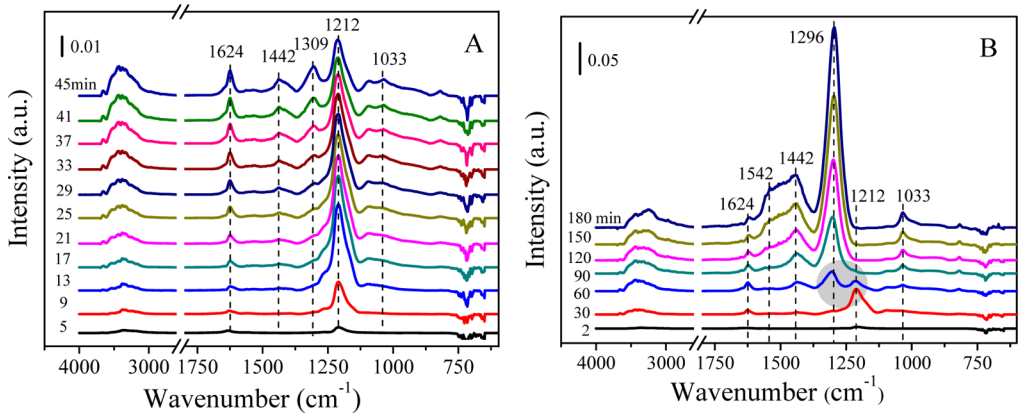

Figure 7. In situ DRIFT spectra of the MnO_x catalyst under an atmosphere of 500 ppm of NO + 5 vol % O_2/Ar (50 mL/min) at 50 °C and (A) 5−45 min and (B) 2−180 min.

addition to an obvious NO_x desorption peak at 103 °C, there were two weak NO_x desorption peaks at 225 and 360 °C, which could be assigned to the decomposition of bridged nitrate and bidentate nitrate species, respectively. For the desorption peak of NO_x at ∼103 °C, the introduction of Sm can enhance its peak area, which corresponds to the amount of weakly adsorbed NO_x, monodentate nitrate and bridged nitrite species on the surface. That is to say, more nitrate/nitrite species on the Sm-MnO_x surface in comparison to those on the surface of MnO_x can participate in the SCR reaction at lower temperature, resulting in an increase in the catalytic activity of the Sm-MnO_x catalyst. In comparison with the Sm-Mn-0.3 catalyst, more nitrate species can adsorb on the surface of the Sm-Mn-0.1 catalyst and take part in the SCR reaction, so that the Sm-Mn-0.1 catalyst exhibited higher SCR activity than the Sm-Mn-0.3 catalyst.

3.4. NO and NH_3 Oxidation. It was reported that improving the catalytic properties of the SCR catalyst for the NO oxidation to NO_2 can significantly promote its low-temperature SCR activity, due to the occurrence of "fast SCR": $NO + NO_2 + 2NH_3 \rightarrow 2N_2 + 3H_2O$.[20,21] Here, the effect of adding Sm on the NO oxidation activity of the MnO_x catalyst

DOI: 10.1021/acscatal.5b00747
ACS Catal. 2015, 5, 5973−5983

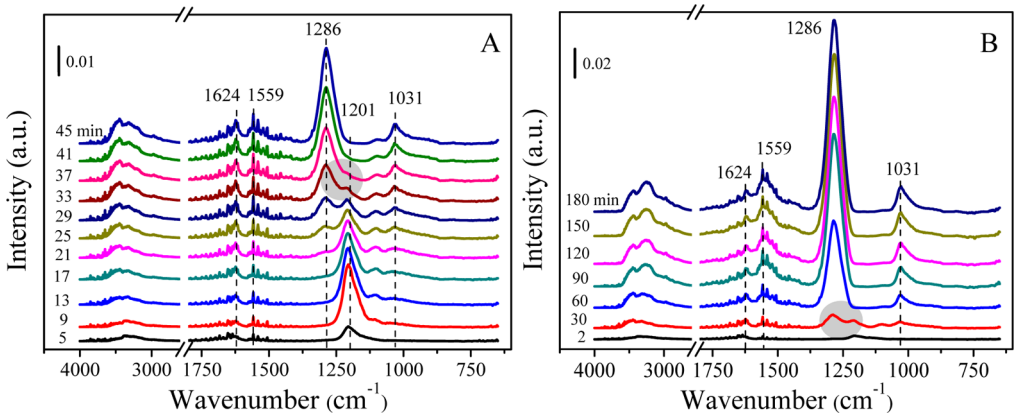

Figure 8. In situ DRIFT spectra of the Sm-Mn-0.1 catalyst under an atmosphere of 500 ppm of NO + 5 vol % O_2/Ar(50 mL/min) at 50 °C and (A) 5−45 min and (B) 2−180 min.

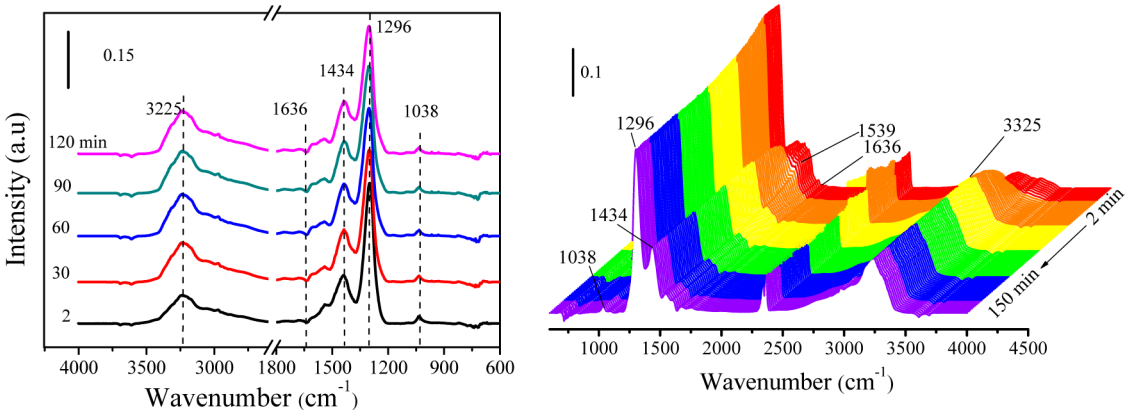

Figure 9. In situ DRIFT spectra of the MnO_x catalyst under an atmosphere of 500 ppm of NH_3/Ar at different times after adsorption of 500 ppm of NO + 5 vol % O_2/Ar at 50 °C and flowing of Ar for 1 h.

was also investigated, and the results are shown in Figure 6. For the NO oxidation at low temperature (<275 °C) (Figure 6A), the catalytic activity of Sm-Mn-0.1 was much closer to that of MnO_x. In contrast, with an increase in the amount of Sm, the catalytic activity of Sm-Mn-0.3 was slightly lower than that of the MnO_x catalyst. On comparison of the NO oxidation by O_2 to NO_2 with the SCR reaction over the Sm-Mn-*X* catalysts (Figure 1), a direct correspondence between their activities for the NO oxidation to NO_2 and the SCR reaction cannot be observed. The reason is that the oxidation of NO to NO_2 (or NO activation) is not the rate-determining step in the SCR reaction over these catalysts,[27,28] and in the NO oxidation the decomposition of nitrate/nitrite species produced by NO oxidation or NO_2 desorption on the catalysts surface was the rate-determining step.[29] In the low-temperature SCR reaction on the Sm-Mn-0.1 catalyst, the oxidation of nitrite species to nitrate and the reaction between the nitrate and NH_3 (or adsorbed) species may be the rate-determining step.

Since NO is one of the byproducts generated during NH_3 oxidation at high temperature, a single NH_3 oxidation was tested on the catalysts. As shown in Figure 6B, for the NH_3 oxidation, the catalytic activity at <300 °C decreases in the order MnO_x > Sm-Mn-0.3 > Sm-Mn-0.1, which indicates that NH_3 oxidation over the MnO_x catalyst under the SCR conditions can be effectively inhibited by the presence of Sm in the MnO_2 catalyst.

3.5. In Situ DRIFT Spectroscopy. *3.5.1. Adsorption of NO + O_2 Followed by Introduction of NH_3.* Prior to the adsorption of NO + O_2, the catalyst was pretreated at 450 °C in Ar (50 mL/min) for 2 h. After the catalyst was cooled to 50 °C, the Ar gas was replaced by the mixed gas of 500 ppm of NO + 5 vol % O_2/Ar (50 mL/min), and in situ DRIFT spectra of the catalyst were taken at different times; the results of MnO_x and Sm-Mn-0.1 catalysts are shown in Figures 7 and 8, respectively.

As shown in Figure 7, six bands at 1624, 1542, 1442, 1309/1296, 1212, and 1033 cm^{-1} appeared, and the bands at 1624, 1442, and 1033 cm^{-1} were assigned to bridged nitrate,[4,30,31] ionic nitrate,[32] and monodentate nitrate,[31,33,34] respectively. The bands at 1542 and 1309/1296 cm^{-1} were assigned to bidentate nitrate,[30,35] and the band at 1212 cm^{-1} was attributed to bridged nitrite.[4,35] It is noted that the band at 1212 cm^{-1} increased first, then decreased with an increase in the adsorption time, and disappeared after 90 min of flowing the mixed gas of NO + O_2. However, the bands at 1309 (shifted to 1296 cm^{-1} with an increase in flow time) and 1542 cm^{-1} appeared after the flow of NO + O_2 for 30 min and increased continually with flowing time until 180 min. These results indicate that NO species may be adsorbed on the surface of the MnO_x catalyst in the form of bridged nitrite at first, and then bridged nitrite was slowly oxidized to bidentate nitrate with more stability, in which the active sites could be released, while NO could adsorb on the released active site to form bidentate nitrate, resulting in the distinct increase in the absorption bands corresponding to nitrate species, such as bidentate nitrate at 1309 cm^{-1} (shifted to 1296 cm^{-1} with an increase in the flow time).

DOI: 10.1021/acscatal.5b00747
ACS Catal. 2015, 5, 5973−5983

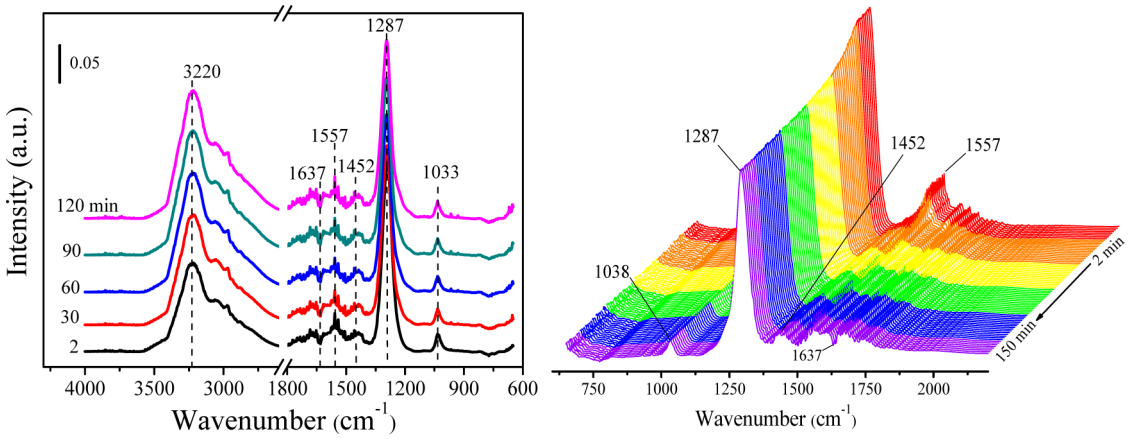

Figure 10. In situ DRIFT spectra of the Sm-Mn-0.1 catalyst under an atmosphere of 500 ppm of NH_3/Ar at different times after adsorption of 500 ppm of NO + 5 vol % O_2/Ar at 50 °C and flowing of Ar for 1 h.

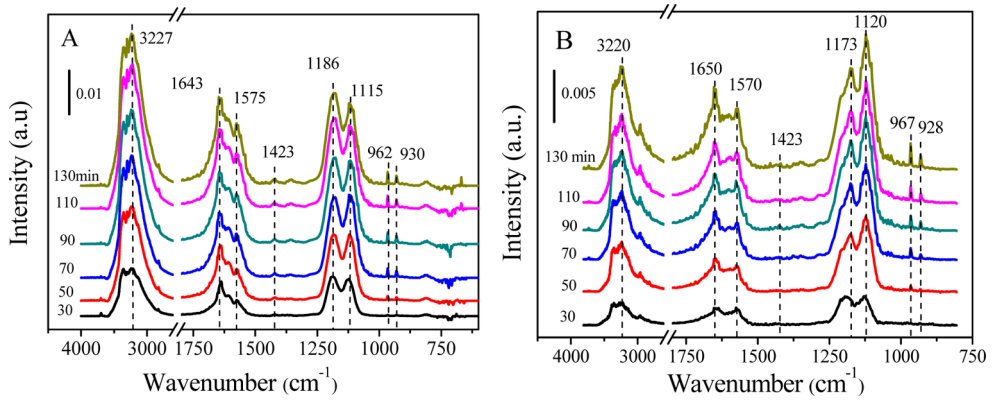

Figure 11. In situ DRIFT spectra of (A) MnO_x and (B) Sm-Mn-0.1 catalysts under an atmosphere of 500 ppm of NH_3/Ar (50 mL/min) at different times.

In comparison with the in situ DRIFT spectra of the MnO_x catalyst, the absorption band of bridged nitrates at 1624 cm^{-1} and the band of monodentate nitrate at 1031 cm^{-1} still existed in the in situ DRIFT spectra of the Sm-Mn-0.1 catalyst (Figure 8), and a small band around 1559 cm^{-1} assigned to bidentate nitrate[34] formed immediately when NO + O_2 flow passed through the catalyst and was enhanced gradually with an increase in the flow time. However, the band at 1201 cm^{-1} assigned to bridged nitrite disappeared after the flow of NO + O_2 for 37 min, and a new band at 1286 cm^{-1} assigned to bidentate nitrate started to appear after 25 min and was enhanced more and more with an increase in the flow time. The band at 1201 cm^{-1} over the MnO_x catalyst disappeared until about 90 min of passing gas. This result shows that bridged nitrite is more easily changed to bidentate nitrate over the Sm-Mn-0.1 catalyst, due to its higher oxidation ability originating from the high Mn^{4+}/Mn^{3+} ratio and more surface oxygen species on the surface of the Sm-MnO_x catalysts. Since bidentate nitrates are the reactive species for the SCR reaction, the high reactivity of the Sm-Mn-0.1 catalyst for the transformation of bridged nitrite to bidentate nitrate would result in its better SCR activity in comparison to the MnO_x catalyst.

After the experiments of Figure 7 (or Figure 8) were finished, the Ar gas (50 mL/min) was used to flow the catalyst instead of the mixed gas of NO + O_2 for 1 h, and then the Ar gas was replaced by 500 ppm of NH_3/Ar, while in situ DRIFT spectra of the catalyst were taken at different times, as shown in Figure 9 over MnO_x (or in Figure 10 over Sm-Mn-0.1).

As shown in Figure 9, the intensity of the bands at 1296 and 1539 cm^{-1} assigned to bidentate nitrate decreased with an increase in the exposure time in 500 ppm of NH_3, whereas the intensities of the bands at 1636 and 1038 cm^{-1} assigned to bridged nitrate and monodentate nitrate were hardly changed, indicating that bidentate nitrates were the most reactive species for SCR reaction. On the other hand, it was surprising that the intensity of the band at 1434 cm^{-1} ascribed to ionic nitrate[32] increased slightly with an extension of the exposure time of NH_3 in initial period, due to the overlapping of NH_3 adsorbed.

In the in situ DRIFT spectra of the Sm-Mn-0.1 catalyst shown in Figure 10, the band at 3225 cm^{-1} was ascribed to the N−H stretching vibration modes of coordinated NH_3,[36] and the bands at 1637 and 1033 cm^{-1} were assigned to bridged nitrate[33,34] and monodentate nitrate,[31,33,34] respectively. Like the DRIFT results of MnO_x, the bands at 1287 and 1557 cm^{-1} were assigned to bidentate nitrate and their intensities decreased with an increase in the exposure time of NH_3, and the variations of other bands with time were not obvious. Different from the DRIFT results of MnO_x, the intensity of the band at 1452 cm^{-1} assigned to ionic nitrate[32] over the Sm-Mn-0.1 catalyst was very low and hardly changed.

3.5.2. Adsorption of NH_3 Followed by Introduction of NO + O_2. Prior to NH_3 adsorption, the MnO_x (or Sm-Mn-0.1) catalyst was pretreated at 450 °C iunder an Ar flow of 50 mL/

DOI: 10.1021/acscatal.5b00747
ACS Catal. 2015, 5, 5973−5983

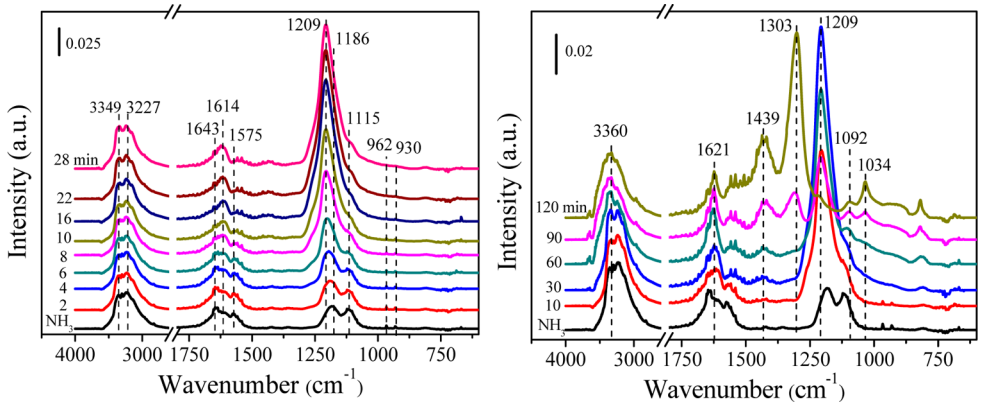

Figure 12. In situ DRIFT spectra of the MnO_x catalyst under an atmosphere of 500 ppm of NO + 5 vol % O_2/Ar at different times after adsorption of 500 ppm of NH_3/Ar at 50 °C and flowing of Ar for 1 h and (A) 2−28 min and (B) 10−120 min.

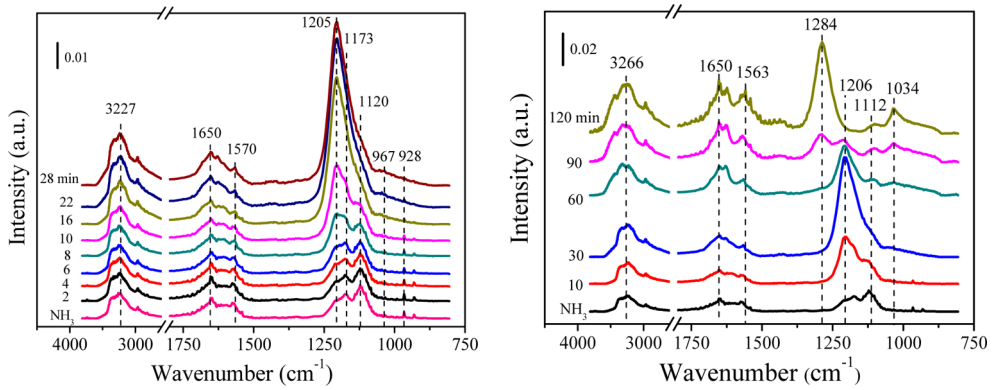

Figure 13. In situ DRIFT spectra of the Sm-Mn-0.1 catalyst under an atmosphere of 500 ppm of NO + 5 vol % O_2/Ar at different times after adsorption of 500 ppm of NH_3/Ar at 50 °C and flowing of Ar for 1 h and (A) 2−28 min and (B) 10−120 min.

min for 2 h and cooled to 50 °C, and then the catalyst was exposed to an atmosphere of 500 ppm of NH_3/Ar (50 mL/min) at 50 °C, while in situ DRIFT spectra of the MnO_x (or Sm-Mn-0.1) catalyst were taken at different times; the results of MnO_x and Sm-Mn-0.1 catalysts are shown in Figure 11.

In the in situ DRIFT spectra of MnO_x shown in Figure 11A, the bands at 930 and 962 cm^{-1} were assigned to gas-phase or weakly adsorbed ammonia,[37] the bands at 1115, 1186, and 1575 cm^{-1} were assigned to NH_3 adsorbed on Lewis acid sites, and the bands at 1423 and 1643 cm^{-1} were correlated to NH_4^+ ions located on Brønsted acid sites.[38−41] The band at 3227 cm^{-1} was ascribed to N−H stretching vibration modes of coordinated NH_3. With an increase in the exposure time, the intensities of all the bands increased markedly, indicating an increase in the amount of adsorbed NH_3 species.

As for the Sm-Mn-0.1 catalyst (Figure 11B), like the in situ DRIFT spectra of the MnO_x catalyst, its gas-phase or weakly adsorbed ammonia (bands at 928 and 967 cm^{-1}), coordinated NH_3 adsorbed on Lewis acid sites (bands at 1120, 1173, and 1570 cm^{-1}), and NH_4^+ ions located on Brønsted acidic sites (band at 1423 and 1650 cm^{-1}) were present, and their intensities increased markedly with an increase in the exposure time of NH_3. In comparison with the bands at 1643 and 1575 cm^{-1} over the MnO_x catalyst (Figure 11A), the relative intensities of bands at 1650 and 1570 cm^{-1} over the Sm-Mn-0.1 catalyst were decreased; furthermore, there was a band at ~1423 cm^{-1} correlated with NH_4^+ ions formed on Brønsted acidic sites of MnO_x, and for Sm-Mn-0.1 this band could not be found. These situations above show that the ratio of B-acid sites to L-acid sites (B/L) over the MnO_x catalyst is higher than that over the Sm-Mn-0.1 catalyst. Since both ionic NH_4^+ and coordinated NH_3 can take part in the SCR process,[42] the proper proportion of B/L over the Sm-Mn-0.1 catalyst may be responsible for its higher SCR activity at lower temperature.[43]

After the experiments of Figure 11 were finished, the Ar gas (50 mL/min) was used to flow the catalyst instead of the mixed gas of NH_3/Ar for 1 h, and then the Ar gas was replaced by 500 ppm of NO + 5 vol % O_2/Ar (50 mL/min), while in situ DRIFT spectra of the catalyst were taken at different times, as shown in Figure 12 over MnO_x (or in Figure 13 over Sm-Mn-0.1).

As shown in Figure 12, the bands at 1643, 1575, 1186, and 1115 cm^{-1} disappeared gradually with an increase in the exposure time of NO + O_2, which indicate that both ionic NH_4^+ and coordinated NH_3 have taken part in the SCR process. However, the bands at 1209, 1303, 1439, and 1621 cm^{-1} assigned to various nitrate and nitrite species appeared and increased with an increase of the exposure time in NO + O_2. When the exposure time of NO + O_2 reached 90 min, the DRIFT absorption spectrum is similar to that of the MnO_x catalyst in the mixed gases of NO + O_2 (Figure 7). After 120 min of passing the gases of NO + O_2, the band of bridged nitrite at 1209 cm^{-1} disappeared completely and only the band of bidentate nitrate at 1303 cm^{-1} could be observed, due to the transition of bridged nitrite to bidentate nitrate, which was also observed in in situ DRIFT spectra of the MnO_x catalyst during the adsorption of NO + O_2 (Figure 7).

DOI: 10.1021/acscatal.5b00747
ACS Catal. 2015, 5, 5973−5983

After Sm (Sm/Mn = 0.1) was added to the MnO_x catalyst, the in situ DRIFT spectra of Figure 13 were obtained. Like the in situ DRIFT spectra over the MnO_x catalyst, the bands at 1173 and 1120 cm^{-1} disappeared gradually with the exposure time, indicating that NH_3 adsorbed on Lewis acid sites has taken part in the SCR process. However, the band at 1570 cm^{-1} (NH_3 on L-acid sites) did not change obviously within 30 min and the intensity of the bands at 1650 cm^{-1} (NH_4^+ ions on B-acid sites) increased; on further increase in the exposure time the band at 1570 cm^{-1} was enhanced gradually, because of the overlapping of nitrate generated. According to in situ DRIFT spectra of the MnO_x catalyst in Figure 12 and other relative research results,[43,44] it can be proposed that the NH_4^+ ions on the B-acid sites of Sm-Mn-0.1 catalyst took part in the SCR reaction. The band at 1205 cm^{-1} assigned to the bridged nitrite increased first and then decreased due to its transformation to bidentate nitrate at 1284 cm^{-1} with an increase in exposure time of NO + O_2. When the exposure time reached 120 min, the DRIFT absorbed spectrum was similar to that of the Sm-Mn-0.1 catalyst in the mixed gas of NO + O_2 (Figure 8).

3.6. Effect of SO_2 and H_2O on the SCR Reaction. Figure 14 shows the influence of SO_2 and H_2O on the activities of the MnO_x and Sm-Mn-0.1 catalysts for the SCR reaction at 100 °C, and the NO_x conversion was ~100% initially over both catalysts. For the MnO_x catalyst, when 2% H_2O was introduced into the feed gas, NO_x conversion decreased to 96% within 10 h, and after removal of the 2% H_2O in the feed gas and continuing for 2 h, the NO_x conversion returned to ~100%. When 50 ppm of SO_2 was added to the feed gas, the 100% NO_x conversion was maintained over the MnO_x catalyst for 8 h. In addition, adding 100 ppm of SO_2 in the feed gas markedly affected the SCR activity of the MnO_x catalyst, which resulted in a decrease in the NO_x conversion from 99% to 82% after 14 h of the reaction. Subsequently, 2% H_2O was simultaneously introduced into the feed gas with 100 ppm of SO_2, while the NO_x conversion decreased from ~82% to ~71%. After both H_2O and SO_2 were removed in the feed gas, the NO_x conversion could recover to 78%.

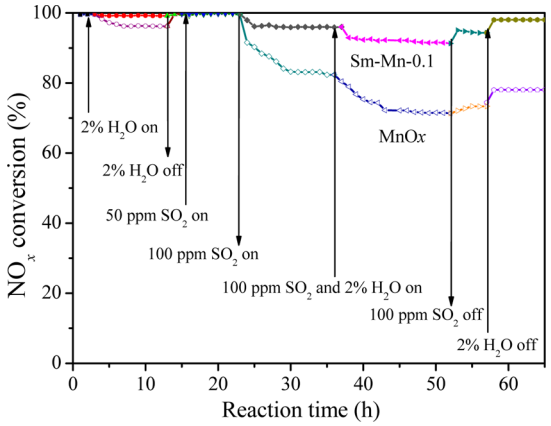

Figure 14. Effect of H_2O and SO_2 on the catalytic activities of the MnO_x and Sm-Mn-0.1 catalysts for the SCR reaction at 100 °C. Reaction conditions: 0.3 g of catalyst, 500 ppm of NO, 500 ppm of NH_3, 5% O_2, Ar to balance, GHSV = 49000 h^{-1}.

In comparison with the MnO_x catalyst, the Sm-Mn-0.1 catalyst exhibited better performance for sulfur resistance and H_2O resistance. The presence of 2% H_2O or 50 ppm of SO_2 did not influence the SCR activity of the Sm-Mn-0.1 catalyst. Although the NO_x conversion decreased to 96% after 14 h of the reaction in the feed gas containing 100 ppm of SO_2, the activity of the Sm-Mn-0.1 catalyst was much higher than that of the MnO_x catalyst after the reaction under the same conditions. Over the Sm-Mn-0.1 catalyst, when using the feed gas containing 2% H_2O and 100 ppm of SO_2, the NO_x conversion remained at about 91%; after both H_2O and SO_2 were removed from the feed gas, the NO_x conversion recovered to 97%, which shows that the Sm-Mn-0.1 catalyst is a much better catalyst than the MnO_x catalyst for the SCR reaction. In addition, the effect of the amount of water (7500 ppm to 2%) on the catalytic performance of Sm-Mn-0.1 at 100 °C was tested. The results show that an NO conversion of ~100% could be maintained when the water concentration in the reactant gas was varied from 7500 ppm to 2% (Figure S5 in the Supporting Information).

The results mentioned above show that H_2O has a less negative influence on the activity of both the MnO_x and Sm-Mn-0.1 catalysts than SO_2 for the SCR reaction, and the Sm-Mn-0.1 catalyst exhibits better performance for sulfur resistance and H_2O resistance than the MnO_x catalyst. When the feed gas contained SO_2, sulfate formed on the catalyst surface to cover the active sites, which was proven by IR experimental results (Figure.S3 in the Supporting Information). In the MnO_x catalyst, the introduction of Sm can induce the formation of bulklike sulfate on Sm_2O_3, which can inhibit the poisoning effect of SO_2 on the active sites of MnO_x.[45]

3.7. Discussion. It was reported that manganese oxides possessed high activity for NH_3-SCR at low temperature.[2,20,21,46,47] Herein, the MnO_x prepared by the precipitation method showed higher activity; for instance, 60% NO_x conversion can be achieved at 50 °C and NO_x can be almost completely reduced at 100 °C. After a certain amount of Sm was introduced into MnO_x its activity could be improved obviously; for instance, the reaction temperature for 100% NO_x conversion can decrease to 75 °C and the operation temperature window can be greatly enlarged. At 25 and 32 °C, the TOF values of catalysts for the SCR reaction were estimated on the basis of their surface concentrations obtained from the XPS data and BET surface area (Table S1 in the Supporting Information), and TOF values were obtained at 25 °C in the order MnO_x (0.87×10^{-4} s^{-1}) < Sm-Mn-0.1 (1.29×10^{-4} s^{-1}) < Sm-Mn-0.3 (1.86×10^{-4} s^{-1}) and at 32 °C in the order MnO_x (1.75×10^{-5} s^{-1}) < Sm-Mn-0.3 (2.18×10^{-4} s^{-1}) < Sm-Mn-0.1 (2.43×10^{-4} s^{-1}), which showed clearly that the presence of Sm can increase the TOF value and improve effectively the catalytic performance of the Mn catalyst. In addition, the Sm-Mn-0.1 catalyst exhibited a high performance for sulfur resistance and H_2O resistance in comparison with the MnO_x catalyst. Therefore, the Sm-Mn-0.1 catalyst may be a potential catalyst for commercial utilization.

We are interested in the promotional mechanism of Sm in the MnO_x catalyst. Sm is prone to insert into the defects of MnO_x, and the introduction of Sm into MnO_x reduced the crystallization of MnO_x, which inhibited the diffusion of Mn^{n+} and O^{2-} ions and prevent the transition of Mn^{4+} to Mn^{3+}, resulting in the high relative contents of both Mn^{4+} and surface oxygen (O_S) on the surface of the Sm-Mn-0.1 catalyst (Figure 4 and Table.1). The relatively high contents of Mn^{4+} and O_S are beneficial for the improvement of the oxidation ability of the Sm-MnO_x catalysts and can enhance the oxidation of bridged nitrite adsorbed on the surface of the Sm-MnO_x catalyst to bidentate nitrate, as shown in in situ DRIFT spectra (Figures 7

DOI: 10.1021/acscatal.5b00747
ACS Catal. 2015, 5, 5973−5983

and 8), which significantly promotes the activity of the Sm-Mn-0.1 catalyst for the SCR reaction at low temperature since the bidentate nitrates are the most reactive species for the SCR reaction.

Further, the relatively high content of Mn^{4+} means that more empty orbitals exist and more Lewis acid sites can be created (Figure 11), which is propitious for the absorption of NH_3 on the Sm-Mn-0.1 catalyst. At the same time, the surface area of the MnO_x catalyst can be effectively enhanced by the presence of an adequate amount of Sm. On the basis of two favorable factors, the amount of adsorbed NH_3 species on the Sm-Mn-0.1 catalyst can be enhanced as indicated by NH_3-TPD. Similarly, the introduction of Sm can promote the NO adsorption as nitrate species at low temperature (<300 °C) (Figure 5), probably due to the increase in its surface area and the ability to convert NO species adsorbed, which are beneficial in promoting the SCR activity of the Sm-Mn-0.1 catalyst. However, if an excess amount of Sm was added to the MnO_x catalyst, as for the Sm-Mn-0.3 catalyst, all these beneficially promotional factors (the surface area and the Mn^{4+}/Mn^{3+} atomic ratio) would be weakened, resulting in a decrease in its catlytic activity for the NH_3-SCR reaction, in comparison with the Sm-Mn-0.1 catalyst.

There is a great difference in the reaction mechanism of the SCR reaction over other Mn-based catalysts. Jin et al.[45] thought that the SCR reaction catalyzed by Lewis acid sites over the Mn/TiO_2 catalyst occurred on the basis of a Langmuir−Hinshelwood mechanism. Yang et al.[20] studied systematically the SCR reaction mechanism over the $Fe_xMn_{3-x}O_4$ catalyst by in situ DRIFT and kinetic studies and indicated that the SCR reaction over the $(Fe_{3-x}Mn_x)_{1-\delta}O_4$ catalyst followed both Eley−Rideal and Langmuir−Hinshelwood mechanisms. However, with a further increase in the Mn amount in the catalyst, an Eley−Rideal mechanism predominated over $(Fe_{2.5}Mn_{0.5})_{1-\delta}O_4$. Kijlstra et al.[48] studied the mechanism of NH_3-SCR at low temperature over the MnO_x/Al_2O_3 catalyst and proposed that NH_3 first adsorbed on the Lewis acid sites and subsequently transformed to NH_2. Ultimately NH_2 reacted with gas-phase NO (E-R mechanism) and nitrite intermediates on the surface (L-H mechanism).

In this paper, we have shown that NO species could adsorb on the surface of the MnO_x and Sm-Mn-0.1 catalysts in the main form of bridged nitrite at first, and then bridged nitrite slowly oxidized to bidentate nitrate, as shown in Figures 7 and 8. Furthermore, the presence of Sm can promote the transformation of nitrite species to nitrates. It was reported that bidentate nitrate resulted from the further oxidization of nitrite.[44] The results in Figure S4 in the Supporting Information show that the nitrite species do not participate in the SCR reaction, while the bidentate nitrates are the active intermediates and can react with NH_3 (Figures 9 and 10). However, it is noticeable from Figures 9 and 10 that the intensities of bands assigned to bidentate nitrate decreased to a certain degree with an increase in the exposure time of NH_3; that is, the majority of bidentate nitrate still remained on the catalyst surface, which cannot be reduced by gaseous NH_3 at 50 °C. These results revealed that the SCR reaction over the MnO_x and Sm-Mn-0.1 catalysts followed a Langmuir−Hinshelwood mechanism. On the other hand, NH_3 could adsorb on both Lewis acid sites and Brønsted acid sites on the MnO_x and Sm-Mn-0.1 catalysts (in situ DRIFT results in Figure 11), and then react with NO species. As a result, the corresponding bands in the in situ DRIFT spectra (Figures 12 and 13) disappeared rapidly when the catalysts pretreated with NH_3 were exposed to the gas mixture of NO and O_2.

As mentioned above, the reaction of NH_3 with the preadsorbed NO + O_2 was very slow, whereas the reaction of NO + O_2 with the preadsorbed NH_3 was rapid over the MnO_x-based catalysts. Therefore, if preadsorbed NH_3 reacted with surface adsorption species of NO in Figures 12 and 13, NH_3 should react with the preadsorbed NO + O_2 more easily, since the adsorption of NH_3 was obligatory for the NH_3-SCR reaction. However, Figures 9 and 10 show that the reaction of NH_3 with the preadsorbed NO + O_2 is slow. Therefore, an E-R mechanism of the NH_3-SCR on the MnO_x and Sm-Mn-0.1 catalysts can be proposed. On the basis of the above discussion, it can be concluded that the NH_3-SCR reaction over the MnO_x and Sm-Mn-0.1 catalysts follows both Eley−Rideal and Langmuir−Hinshelwood mechanisms, in which the Eley−Rideal mechanism predominated.

4. CONCLUSIONS

In summary, highly efficient Sm-MnO_x catalysts for the SCR reaction at low temperature were prepared by the coprecipitation method. The results show that an introduction of a proper amount of Sm into the MnO_x catalyst can markedly improve its catalytic activity for NH_3-SCR and increase its abilities for sulfur resistance and H_2O resistance. For instance, NO_x could be completely converted at 75 °C and the operation temperature window was greatly enlarged over the Sm-Mn-0.1 (Sm/Mn = 0.1 (mol)) catalyst; the presence of 2% H_2O or 50 ppm of SO_2 in the feed gas would not affect the SCR activity of the Sm-Mn-0.1 catalyst. When the feed gas contained 2% H_2O and 100 ppm of SO_2, the NO_x conversion remained at 91% at 100 °C.

The introduction of Sm into MnO_x can increase the relative content of Mn^{4+} and surface oxygen (O_S) on the surface of Sm-Mn-0.1 catalyst, promoting the oxidation of bridged nitrite adsorbed on the Sm-MnO_x catalyst surface to bidentate nitrate. In comparison with the MnO_x catalyst, the Sm-Mn-0.1 catalyst has higher specific surface area and more surface defects, which helps to increase the absorption amount of NH_3 and NO on the Sm-Mn-0.1 catalyst. These factors above can promote the catalytic performance of the Sm-Mn-0.1 catalyst. When an excess amount of Sm was added to the MnO_x catalyst, such as Sm-Mn-0.3 catalyst, all these beneficial factors above would be weakened, resulting in a decrease in the catalytic activity for NH_3-SCR in comparison with the Sm-Mn-0.1 catalyst.

The in situ DRIFT results showed that NH_3 adsorbed on both Lewis acid sites and Brønsted acid sites on the Sm-Mn-0.1 surface can easily react with NO_x gas. The NO species can adsorb on the Sm-Mn-0.1 surface in the form of bridged nitrite, and then bridged nitrite slowly oxidized to bidentate nitrate, which is the active intermediate for the NH_3-SCR reaction. At low temperature (as 50 °C), only highly active bidentate nitrate can be reduced by gaseous NH_3, and the majority of bidentate nitrate still remained on the catalyst surface. Therefore, we can conclude that the SCR reaction over the Sm-Mn-0.1 catalyst follows both Eley−Rideal and Langmuir−Hinshelwood mechanisms, of which the Eley−Rideal mechanism is predominant.

■ ASSOCIATED CONTENT

Supporting Information

The Supporting Information is available free of charge on the ACS Publications website at DOI: 10.1021/acscatal.5b00747.

DOI: 10.1021/acscatal.5b00747
ACS Catal. 2015, 5, 5973−5983

In situ DRIFT spectra of NO-TPD over the MnO_x and Sm-Mn-0.1 catalysts (Figures S1 and S2), the Sm-Mn-0.1 catalyst used in the SCR reaction containing 2% H_2O and 100 ppm of SO_2 (Figure S3) and the Sm-Mn-0.1 catalyst under different atmospheres (Figure S4), the effect of water concentration on the catalytic performance (Figure S5), the calculation method of TOF, and the surface compositions and SCR activity data of catalysts (Table S1). (PDF)

AUTHOR INFORMATION

Corresponding Authors

*W. Zhan: e-mail, zhanwc@ecust.edu.cn.

*G. Lu: fax, +86-21-64252923; e-mail, gzhlu@ecust.edu.cn.

Notes

The authors declare no competing financial interest.

ACKNOWLEDGMENTS

This work was supported financially by the National Natural Science Foundation of China (21577034, 21333003), the National High Technology Research and Development Program of China (2012AA111717), and the Fundamental Research Funds for the Central Universities (WA1514020).

REFERENCES

(1) Sun, L.; Cao, Q.; Hu, B.; Li, J.; Hao, J.; Jing, G.; Tang, X. *Appl. Catal., A* **2011**, *393*, 323−330.

(2) Kang, M.; Park, E. D.; Kim, J. M.; Yie, J. E. *Appl. Catal., A* **2007**, *327*, 261−269.

(3) Forzatti, P. *Appl. Catal., A* **2001**, *222*, 221−236.

(4) Chen, L.; Li, J.; Ge, M. *J. Phys. Chem. C* **2009**, *113*, 21177−21184.

(5) Deka, U.; Lezcano-Gonzalez, I.; Weckhuysen, B. M.; Beale, A. M. *ACS Catal.* **2013**, *3*, 413−427.

(6) Wang, D.; Zhang, L.; Kamasamudram, K.; Epling, W. S. *ACS Catal.* **2013**, *3*, 871−881.

(7) Gao, F.; Walter, E. D.; Washton, N. M.; Szanyi, J.; Peden, C. H. F. *ACS Catal.* **2013**, *3*, 2083−2093.

(8) Kang, M.; Park, E. D.; Kim, J. M.; Yie, J. E. *Catal. Today* **2006**, *111*, 236−241.

(9) Zhou, C.; Zhang, Y.; Wang, X.; Xu, H.; Sun, K.; Shen, K. *J. Colloid Interface Sci.* **2013**, *392*, 319−324.

(10) Roy, S.; Viswanath, B.; Hegde, M.; Madras, G. *J. Phys. Chem. C* **2008**, *112*, 6002−6012.

(11) Peña, D. A.; Uphade, B. S.; Smirniotis, P. G. *J. Catal.* **2004**, *221*, 421−431.

(12) Kapteijn, F.; Singoredjo, L.; Andreini, A.; Moulijn, J. *Appl. Catal., B* **1994**, *3*, 173−189.

(13) Kang, M.; Park, J. H.; Choi, J. S.; Park, E. D.; Yie, J. E. *Korean J. Chem. Eng.* **2007**, *24*, 191−195.

(14) Richter, M.; Trunschke, A.; Bentrup, U.; Brzezinka, K. W.; Schreier, E.; Schneider, M.; Pohl, M. M.; Fricke, R. *J. Catal.* **2002**, *206*, 98−113.

(15) Wang, X.; Zheng, Y.; Lin, J. *Catal. Commun.* **2013**, *37*, 96−99.

(16) Pourkhalil, M.; Moghaddam, A. Z.; Rashidi, A.; Towfighi, J.; Mortazavi, Y. *Appl. Surf. Sci.* **2013**, *279*, 250−259.

(17) Wu, Z.; Jiang, B.; Liu, Y. *Appl. Catal., B* **2008**, *79*, 347−355.

(18) Qi, G.; Yang, R. T.; Chang, R. *Appl. Catal., B* **2004**, *51*, 93−106.

(19) Rodriguez, J. A.; Stacchiola, D. *Phys. Chem. Chem. Phys.* **2010**, *12*, 9557−9565.

(20) Yang, S.; Wang, C.; Li, J.; Yan, N.; Ma, L.; Chang, H. *Appl. Catal., B* **2011**, *110*, 71−80.

(21) Chen, J.; Shen, M.; Wang, X.; Qi, G.; Wang, J.; Li, W. *Appl. Catal., B* **2013**, *134−135*, 251−257.

(22) Shinjoh, H. *J. Alloys Compd.* **2006**, *408-412*, 1061−1064.

(23) Chang, H.; Li, J.; Yuan, J.; Chen, L.; Dai, Y.; Arandiyan, H.; Xu, J.; Hao, J. *Catal. Today* **2013**, *201*, 139−144.

(24) Tang, X.; Li, J.; Sun, L.; Hao, J. *Appl. Catal., B* **2010**, *99*, 156−162.

(25) Wu, Z.; Jin, R.; Liu, Y.; Wang, H. *Catal. Commun.* **2008**, *9*, 2217−2220.

(26) Qiu, M.; Zhan, S.; Yu, H.; Zhu, D.; Wang, S. *Nanoscale* **2015**, *7* (6), 2568−2577.

(27) Janssens, T.; Falsig, H.; Lundegaard, L.; Vennestrom, P.; Rasmussen, S.; Moses, P.; Giordanino, F.; Borfrecchia, E.; Lamachenko, K.; Lamberti, C.; Bordiga, S.; Godiksen, A.; Mossin, S.; Beato, P. *ACS Catal.* **2015**, *5*, 2832−2845.

(28) Ruggeri, M.; Nova, I.; Tronconi, E.; Pihl, J.; Toops, T.; Partridge, W. *Appl. Catal., B* **2015**, *166−167*, 181−192.

(29) Shen, B.; Lin, X.; Zhao, Y. *Chem. Eng. J.* **2013**, *222*, 9−15.

(30) Wang, W.; McCool, G.; Kapur, N.; Yuan, G.; Shan, B.; Nugyen, M.; Graham, U. M.; Davis, B. H.; Jacobs, G.; Cho, K.; Hao, X. *Science* **2012**, *337*, 832−835.

(31) Atribak, I.; Azambre, B.; Bueno López, A.; García-García, A. *Appl. Catal., B* **2009**, *92*, 126−137.

(32) Li, Q.; Meng, M.; Zou, Z.; Li, X.; Zha, Y. Q. *J. Hazard. Mater.* **2009**, *161*, 366−372.

(33) Zhang, Z.; Zhang, Y.; Su, Q.; Wang, Z.; Li, Q.; Gao, X. *Environ. Sci. Technol.* **2010**, *44*, 8254−8258.

(34) Yung, M. M.; Holmgreen, E. M.; Ozkan, U. S. *J. Catal.* **2007**, *247*, 356−367.

(35) Shuang, L.; Wu, X.; Weng, D.; Ran, R. *Ind. Eng. Chem. Res.* **2012**, *51*, 2271−2279.

(36) Shan, W.; Liu, F.; Hong, H.; Shi, X.; Zhang, C. *Appl. Catal., B* **2012**, *115−116*, 100−106.

(37) Gu, T.; Jin, R.; Liu, Y.; Liu, H.; Weng, X.; Wu, Z. *Appl. Catal., B* **2013**, *129*, 30−38.

(38) Liu, F.; He, H. *J. Phys. Chem. C* **2010**, *114*, 16929−16936.

(39) Peña, D. A.; Uphade, B. S.; Reddy, E. P.; Smirniotis, P. G. *J. Phys. Chem. B* **2004**, *108*, 9927−9936.

(40) Topsoe, N.; Topsoe, H.; Dumesic, J. *J. Catal.* **1995**, *151*, 226−240.

(41) Matralis, H. K.; Ciardelli, M.; Ruwet, M.; Grange, P. *J. Catal.* **1995**, *157*, 368−379.

(42) Long, R. Q.; Yang, R. T. *J. Catal.* **2002**, *207*, 224−231.

(43) Liu, F.; He, H.; Ding, Y.; Zhang, C. *Appl. Catal., B* **2009**, *93*, 194−204.

(44) Liu, Z.; Zhang, S.; Li, J.; Ma, L. *Appl. Catal., B* **2014**, *144*, 90−95.

(45) Jin, R.; Liu, Y.; Wang, Y.; Cen, W.; Wu, Z.; Wang, H.; Weng, X. *Appl. Catal., B* **2014**, *148−149*, 582−588.

(46) Wan, Y.; Zhao, W.; Tang, Y.; Li, L.; Wang, H.; Cui, Y.; Gu, J.; Li, Y.; Shi, J. *Appl. Catal., B* **2014**, *148−149*, 114−122.

(47) Qi, G.; Yang, R. T. *J. Catal.* **2003**, *217*, 434−441.

(48) Kijlstra, W. S.; Brands, D. S.; Smit, H. I.; Poels, E. K.; Bliek, A. *J. Catal.* **1997**, *171*, 219−230.

DOI: 10.1021/acscatal.5b00747
ACS Catal. 2015, 5, 5973−5983